

Precise predictions for $W\gamma\gamma$ +jet production at hadron colliders

Francisco Campanario,^{1,*} Christoph Englert,^{2,†} Michael Rauch,^{1,‡} and Dieter Zeppenfeld^{1,§}

¹*Institute for Theoretical Physics, KIT, 76128 Karlsruhe, Germany*

²*Institute for Theoretical Physics, Heidelberg University, 69120 Heidelberg, Germany*

In this letter we report on a calculation of $W^\pm\gamma\gamma$ +jet production at next-to-leading order QCD. We include the leptonic decays of the W and take into account all off-shell and finite width effects. This is the first computation which falls into the category of triboson+jet production at next-to-leading order QCD. In total we find sizable corrections with nontrivial phase space dependencies. Therefore, our results are important for phenomenological analyses such as the extraction of anomalous electroweak quartic couplings from inclusive hadron collider data.

I. INTRODUCTION

The production of multiple electroweak bosons is an important channel to test experimental data, collected at both the Tevatron and the Large Hadron Collider (LHC), against the theoretically well-established Standard Model (SM) hypothesis. As the mechanism of electroweak symmetry breaking is yet to be determined, precise predictions of electroweak gauge boson production rates are necessary to experimentally infer deviations from the electroweak coupling pattern predicted by the SM. It is well-known that computations of production cross sections and differential distributions suffer from severe theoretical shortcomings if they are limited to the semi-classical (*i.e.* leading order, LO) approximation in perturbation theory. The arising uncertainties intrinsic to fixed order calculations are conventionally assessed by investigating variations of renormalization and factorization scales, which are remnants of the perturbative series' truncation.

The next-to-leading order (NLO) real emission contribution to the hadronic cross section, however, can probe new partonic initial states not present at LO, so that the LO scale uncertainty can sometimes be totally misleading. This is especially true for processes which are characterized by a QCD singlet final state at LO, *e.g.*, electroweak triboson production [1, 2]. For these channels the total NLO correction factors are known to be particularly sizable, $K = \sigma^{\text{NLO}}/\sigma^{\text{LO}} \sim 1.8$. The main reason for this large correction is that the NLO corrections include new, large LO real emission subprocesses initiated by gluons. Probing the protons' gluon parton distribution at small momentum fractions with the real emission contribution, the large correction does not signal a breakdown of perturbation theory, but strongly asks for perturbative improvements of the one-jet-inclusive cross sections as a major contribution to the full next-to-next-to-leading order cross sections. Similar observations and

conclusions hold for diboson [3, 4] and diboson+jet production [5–8] (see also Ref. [9] for a related discussion of Z +jets).

In this paper we report on the first calculation performed in the context of triboson + jet production: $p\bar{p} \rightarrow \ell^- \bar{\nu}_\ell \gamma \gamma + \text{jet} + X$ and $p\bar{p} \rightarrow \ell^+ \nu_\ell \gamma \gamma + \text{jet} + X$. We include all off-shell and finite width effects in our calculation, *i.e.* we compute the full matrix element at $\mathcal{O}(\alpha^4 \alpha_s^2)$. For convenience we will refer to these processes as $W^\pm\gamma\gamma$ + jet production.

We organize this paper as follows: Section II reviews the technical details of the calculation and comments on the numerical Monte Carlo implementation. In Sec. III we discuss the numerical results; we examine the cross sections' scale variations and the impact of the QCD corrections on differential distributions. Section IV gives a summary of this work.

II. ELEMENTS OF THE CALCULATION

The leading order $\mathcal{O}(\alpha^4 \alpha_s)$ contribution to, *e.g.*, $p\bar{p} \rightarrow \ell^- \bar{\nu}_\ell \gamma \gamma + \text{jet}$ is given by the subprocesses

$$q\bar{Q} \rightarrow \ell^- \bar{\nu}_\ell \gamma \gamma + g, \quad (1a)$$

$$g\bar{Q} \rightarrow \ell^- \bar{\nu}_\ell \gamma \gamma + \bar{q}, \quad (1b)$$

$$qg \rightarrow \ell^- \bar{\nu}_\ell \gamma \gamma + Q, \quad (1c)$$

where $q = (d, s)$ and $Q = (u, c)$ denote the light down- and up-type quark flavors, respectively. Due to unitarity of the CKM matrix, any dependence on the CKM matrix elements drops out for the flavor-summed gluon-induced subprocesses of Eq. (1b), (1c). These subprocesses also dominate the hadronic cross sections at the LHC because the protons are typically probed at small momentum fractions for inclusive production. Consequently, a non-diagonal CKM matrix decreases our LO result only at the per mill-level. This is well below the residual (NLO) scale uncertainty and we therefore use a diagonal CKM matrix in our calculation. Furthermore, we do not include bottom contributions to the hadronic $W\gamma\gamma$ +jet production cross section. They either involve top or bottom quarks in the final state and are distinguishable experimentally by b tagging.

*Electronic address: francam@particle.uni-karlsruhe.de

†Electronic address: c.englert@thphys.uni-heidelberg.de

‡Electronic address: rauch@particle.uni-karlsruhe.de

§Electronic address: dieter@particle.uni-karlsruhe.de

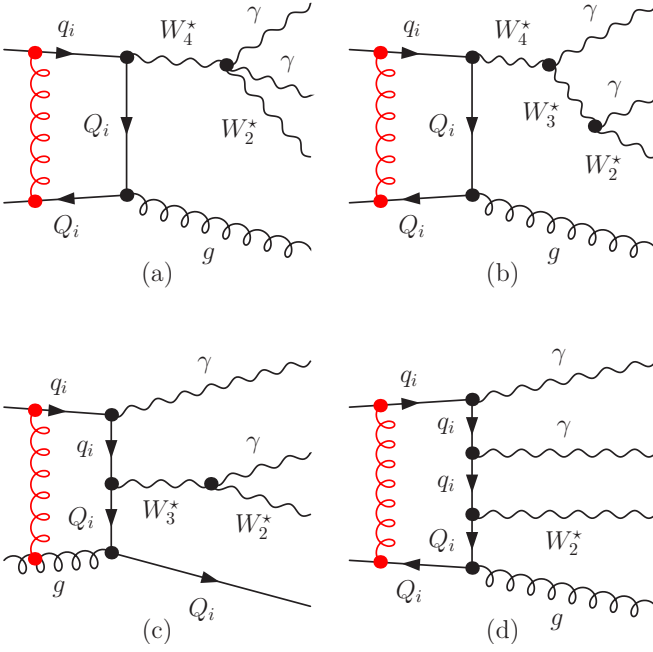


FIG. 1: Selected topologies contributing to $W^- \gamma \gamma + \text{jet}$ production at NLO; $i = 1, 2$ denotes the generation index. Note that we do not show the contributions $W_n^* \rightarrow e^- \bar{\nu}_e + (n-2)\gamma$, $2 \leq n \leq 4$. These lead to identical configurations from the QCD point of view. The red loops indicate the virtual contributions, giving rise to topologies of up to boxes (a,b), up to pentagons (c) and up to hexagons (d).

For the numerical implementation of the LO cross section we use routines that are provided by the VBFNLO package [10] as the real emission contribution to $W \gamma \gamma$ production at NLO QCD [2]. The hadronic part of the amplitude is based on the spinor helicity formalism of Ref. [11], and the electroweak part of the amplitude is provided by a cache system which employs MADGRAPH-generated HELAS routines [12, 13] using the technique of “leptonic tensors” [14]. All amplitudes of Eq. (1) are related by crossing symmetry, and we show a sample of graphs contributing at NLO in Fig. 1.

For the virtual contributions we use the routines computed in Ref. [15] which employ FEYNALC [16] and FEYNARTS [17] in an in-house framework. We apply the effective current approach described in, *e.g.*, Refs. [2, 6, 15, 18], and combine all QCD corrections to sets of topologies with two, three, and four attached (effective) gauge boson polarization vectors to standalone numerical routines.* The order of the gauge bosons is thereby fixed and the full amplitude is obtained by summing over all allowed permutations. The effective W_n^* polarization vectors, see Fig. 1, encode the finite width

effects in the fixed-width scheme of Ref. [21] and the off-shell contributions of the full decays $W_n^* \rightarrow \ell \nu + (n-2)\gamma$, $2 \leq n \leq 4$, in a straightforward way. To be more concrete, Figs. 1 (a) and (b) contribute to a routine which includes all corrections up to boxes (*i.e.* all corrections to $q\bar{Q} \rightarrow W_4^* g$ with terms proportional to C_A and $C_F - \frac{1}{2}C_A$), Fig. 1 (c) is part of a routine which includes corrections up to pentagons ($\bar{Q}g \rightarrow W_3^* \gamma \bar{q}$), and Fig. 1 (d) contributes to a routine which also includes hexagon diagrams ($q\bar{Q} \rightarrow W_2^* \gamma \gamma g$). The fermion loop contributions are sketched in Fig. 2 and were computed within the in-house framework [15] and checked against an independent implementation based on FEYNARTS, FORMCALC and LOOPTOOLS [17, 22, 23].

For the reduction of the tensor coefficients up to boxes we apply the Passarino-Veltman approach of Ref. [24], and for a numerically stable implementation of 5- and 6-point coefficients we use the Denner-Dittmaier scheme laid out in Ref. [25] with the setup and notation of Ref. [15]. This approach has turned out adequate in a series of Feynman graph-based hexagon calculations, *e.g.*, in Ref. [26]. For completeness, we note that unitarity cut-based methods have been demonstrated to be highly competitive in Ref. [27].

The real emission contribution, $p \bar{p} \rightarrow \ell^- \bar{\nu}_\ell \gamma \gamma + 2 \text{jets}$, is based on the existing implementations of Refs. [6, 7]. We use the Catani-Seymour dipole formalism [28] to numerically regularize the soft and collinear QCD divergences and include finite contributions after cancelling the infrared poles of the virtual matrix element [15] to order $\mathcal{O}(\alpha^4 \alpha_s^2)$. The real emission matrix element again implements the spinor-helicity formalism of Ref. [11] and, analogous to the LO amplitude, the implementation includes a cache system for the electroweak W_n^* currents to minimize computation time. The implementation of the dipoles is optimized to avoid redundancy, and the finite

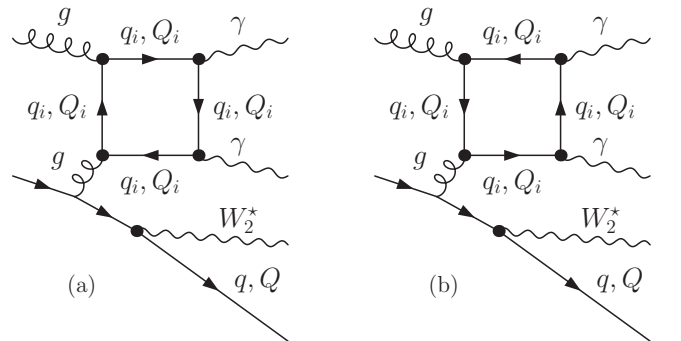


FIG. 2: Fermion loop contributions to $W \gamma \gamma + \text{jet}$ production at NLO; $i = 1, 2, 3$ denotes the generation index. q stands for all (anti)quark flavors of the incoming (anti)proton. Note that analogous $gg\gamma$ triangle contributions are forbidden by Furry’s theorem. Not shown are topologies where the polarization vector W_2^* is attached to the initial state (anti)quark, and where the internal and external gluon are attached at opposite corners of the box.

*This approach allows to straightforwardly generalize our computation to models beyond the Standard Model as described in Refs. [7, 19, 20].

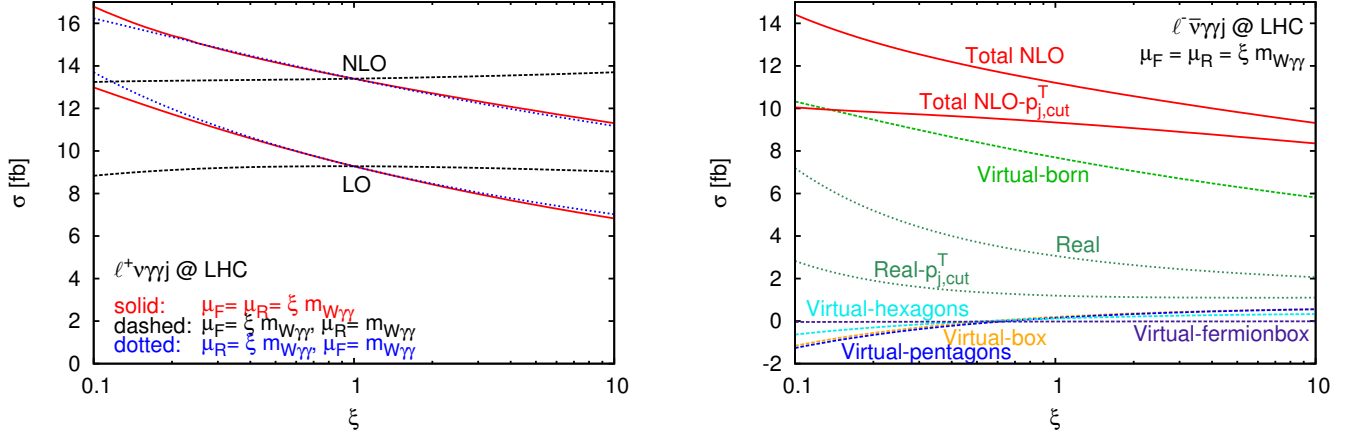


FIG. 3: Scale variation of the $\ell^\pm \nu \gamma \gamma + \text{jet}$ production cross sections at the LHC ($\ell = e, \mu$). The cuts are described in the text and we take the invariant $W\gamma\gamma$ mass $m_{W\gamma\gamma}$ as central dynamical reference scale. The left panel shows the variation of the LO and NLO $W^+ \gamma \gamma + \text{jet}$ production cross sections when we change only the factorization scale, only the renormalization scale, or both jointly. For $W^- \gamma \gamma + \text{jet}$ production the right panel shows the individual contributions to the NLO cross section, as discussed in the text. Here we also present results where we have applied a veto on events with two identified jets having both a transverse momentum larger than 50 GeV.

	σ^{LO} [fb]	σ^{NLO} [fb]	$K = \sigma^{\text{NLO}}/\sigma^{\text{LO}}$	
$W^\pm \gamma \gamma + \text{jet}$	1.191	1.754	1.47	Tevatron
$W^+ \gamma \gamma + \text{jet}$	4.640	6.634	1.43	LHC
$W^- \gamma \gamma + \text{jet}$	3.803	5.644	1.48	

TABLE I: Total LO and NLO cross sections and K factors for $p p \rightarrow e^- \bar{\nu}_e \gamma \gamma + \text{jet} + X$ and $p p \rightarrow e^+ \nu_e \gamma \gamma + \text{jet} + X$ at the Tevatron and at the LHC. The renormalization and factorization scales are chosen as $\mu_R = \mu_F = m_{W\gamma\gamma}$. Relative statistical and numerical stability errors are below the per mill level.

collinear remainder, which is left after renormalizing the parton densities, recycles the born-level matrix elements of the dipoles' evaluation and is integrated over the real emission phase space applying the phase space mappings of Ref. [18].

III. NUMERICAL RESULTS

We use CT10 parton distributions [29] with $\alpha_s(m_Z) = 0.118$ at NLO, and the CTEQ6L1 set [30] with $\alpha_s(m_Z) = 0.130$ at LO. We choose $m_Z = 91.1876$ GeV, $m_W = 80.398$ GeV and $G_F = 1.16637 \times 10^{-5}$ GeV $^{-2}$ as electroweak input parameters and derive the electromagnetic coupling α and the weak mixing angle from Standard Model-tree level relations. The center-of-mass energy is fixed to 14 TeV for LHC and 1.96 TeV for Tevatron collisions, respectively. We consider W^\pm decays to the two light lepton flavors, *i.e.* for the distributions shown in Figs. 3-6 the decays $W \rightarrow e \nu_e, \mu \nu_\mu$ have been summed, and we treat these leptons as massless.

To study the impact of the QCD corrections on the process in detail, we choose very inclusive cuts and a strictly isolated photon. A naive isolation criterion for the partons and the photon spoils infrared safety by limiting the soft gluon emissions' phase space. Yet, isolation is necessary to avoid non-perturbative jet-fragmentation contributions, which would amount to the introduction of an additional fragmentation scale to the problem. Instead, we apply the prescription suggested in Ref. [31] (see also Ref. [32]), demanding

$$\sum_{i, R_{i\gamma} < R} p_T^{\text{parton}, i} \leq \frac{1 - \cos R}{1 - \cos \delta_0} p_T^\gamma \quad \forall R \leq \delta_0, \quad (2)$$

where the index i runs over all partons in a cone around the photon of size R . For the cut-off parameter, which determines the QCD-IR-safe cone size around the photon, we choose $\delta_0 = 0.7$. This is a rather large isolation compared to the experimental resolution capabilities (*e.g.* Ref. [33]). Hence, the phenomenological impact of the full jet-photon fragmentation is expected to be small, in accordance with the results of Refs. [7, 34, 35].

We cluster all final state partons with $|y_p| \leq 5$ to jets via the k_T algorithm [36] using a resolution parameter $D = 0.8$, adding the four momenta of clustered partons. The jets are required to lie in the rapidity range $|y_j| \leq 4.5$ with transverse momenta $p_T^j \geq 20$ GeV. The photon and the charged lepton are required to be hard and central, $p_T^\ell \geq 20$ GeV (10 GeV at the Tevatron), $p_T^\gamma \geq 20$ GeV (10 GeV at the Tevatron), $|\eta_\ell|, |\eta_\gamma| \leq 2.5$, while being separated in the azimuthal angle-pseudorapidity plane by $R_{\ell\gamma} = (\Delta\phi_{\ell\gamma}^2 + \Delta\eta_{\ell\gamma}^2)^{1/2} \geq 0.4$. For the separation of the charged lepton from observable jets, we choose $R_{\ell j} \geq 0.4$ and we require $R_{\gamma\gamma} \geq 0.4$ for the diphoton separation.

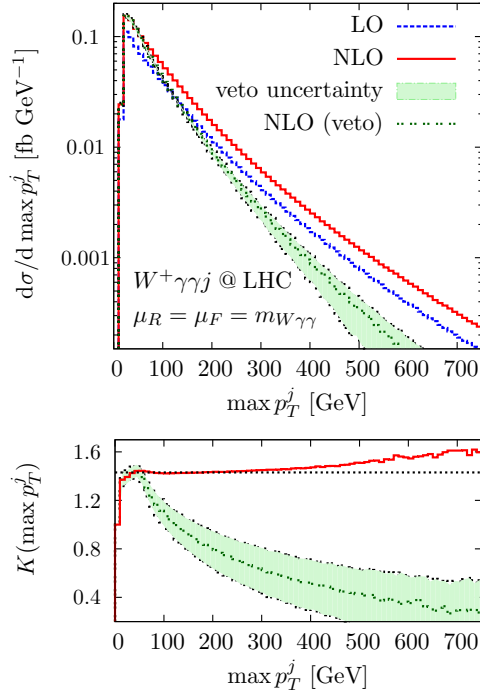


FIG. 4: Differential $\max p_T^j$ distribution for $W^- \gamma \gamma + \text{jet}$ production. The chosen cuts and scales are described in text. The horizontal line in the lower panel displays the K factor for total inclusive production, Tab. I.

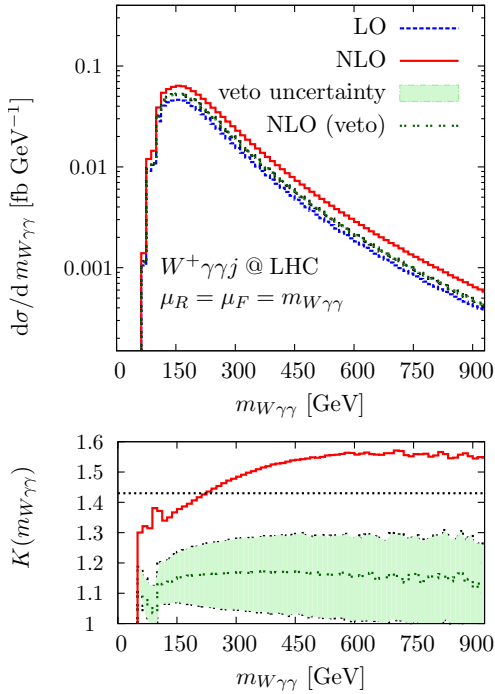


FIG. 5: $W \gamma \gamma$ invariant mass distribution for $W^- \gamma \gamma + \text{jet}$ production. The chosen cuts and scales are described in text. The horizontal line in the lower panel displays the K factor for total inclusive production, Tab. I.

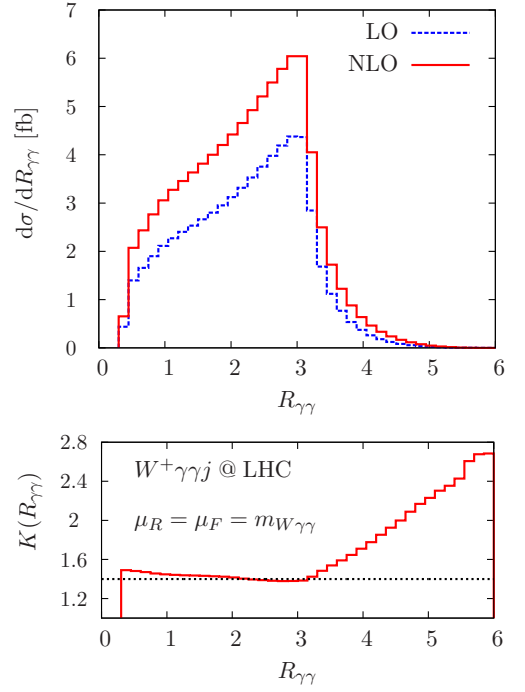


FIG. 6: Differential diphoton R separation distribution for $W^- \gamma \gamma + \text{jet}$ production. The chosen cuts and scales are described in text. The horizontal line in the lower panel displays the K factor for total inclusive production, Tab. I.

Besides the photon-parton isolation criterion mentioned before, we also require a separation between photons and identified jets of $R_{\gamma j} \geq 0.7$. The cross sections and total K factors for a dynamical scale choice $\mu_R = \mu_F = m_{W \gamma \gamma}$ are shown in Tab. I. Here, $m_{W \gamma \gamma}$ denotes the $W^\pm \gamma \gamma$ invariant mass.

The production cross section at the Tevatron is too small to be of evident phenomenological importance when viewed in the light of a total accumulated data set of $\sim 10 \text{ fb}^{-1}$ per experiment.

We compute total K factors of 1.43 (1.48) for $W^+ \gamma \gamma + \text{jet}$ ($W^- \gamma \gamma + \text{jet}$) production at the LHC. These values are quite typical for multiboson+jet production as found in Refs. [5–8]. The scale dependence of the $W^+ \gamma \gamma j$ and $W^- \gamma \gamma j$ production cross sections turn out to be modest: when comparing $\mu_R = \mu_F = \xi m_{W \gamma \gamma}$ for $\xi = 0.5$ and $\xi = 2$, we find differences of 10.8% (12.0%), respectively. The dependence is dominated by the renormalization scale, as can be seen in Fig. 3. This is a consequence of additional jet radiation being important for the probed small gluon momentum fractions. The right panel of Fig. 3 also shows the effect of vetoing a second hard jet. The real contributions become smaller and there is a cut-dependent partial and accidental cancellation within the different contributions, which should not to be taken as a stabilization of perturbation theory, however (see also [7, 8] and below). For the numerical evaluation, we split the virtual contributions into fermionic loops (Virtual-fermionbox, corresponding

to the diagrams sketched in Fig. 2) and bosonic contributions with one, two and three electroweak vector bosons attached to the quark line, *i.e.* Virtual-box, Figs. 1 (a) and (b), Virtual-pentagons, Fig. 1 (c) or Virtual-hexagons, Fig. 1 (d), respectively. This procedure allows us to drastically reduce the time spent in evaluating the part containing hexagon diagrams, which requires the largest amount of CPU time. The bosonic contributions are not individually QED gauge-invariant. However, this poses no problem since for our choice of gauge (effectively, the Coulomb gauge in the lab-frame is used for external photons) there are no sizable cancellations among the different contributions. The fact that in Fig. 3 the different virtual contributions share the same scale dependence corroborates our gauge choice.

The phase space dependence of the QCD corrections is non-trivial and sizable, as can be inferred from Figs. 4-6, where we again choose $\mu_R = \mu_F = m_{W\gamma\gamma}$. Additional parton emission redistributes the transverse momentum spectra. The leading jet becomes slightly harder at NLO, an effect which is best seen in the dynamical K factor (ratio of NLO to LO distribution) as shown in the bottom panel of Fig. 4. The effect on the $W\gamma\gamma$ invariant mass is even more pronounced. While this qualitative behavior is expected from kinematics, *e.g.* due to a photon picking up the recoil from additional parton emission, the quantitative result is very important. An excess in the photon's transverse momentum or in the $W\gamma\gamma$ invariant mass at large values is easily misinterpreted as an effect of anomalous electroweak trilinear or quartic couplings [7, 8, 32] arising from new interactions beyond the SM.

The sizable impact of QCD corrections at large invariant masses is also visible in the diphoton separation of Fig. 6. At large values, when photons are highly separated in pseudorapidity, the dynamical K -factor rises well above the average value of 1.43. This experimentally clean and well-reconstructable configuration typically amounts to a large momentum transfer in the quartic and trilinear vertices in Figs. 1 (a) and (b) and therefore potentially accesses new interactions at scales much larger than m_W .

In Figs. 4 and 5, we also plot distributions with a veto on a second hard jet: no such jet with $p_{T,j} > 50$ GeV is allowed. It can be observed in Fig. 4 that the vetoed contribution does not give a sensible result for large values of p_T of the harder jet, where large logarithms involving

$p_{T,\text{cut}}$ as the other relevant scale appear: changing values from $\mu_R = \mu_F = 1/2m_{W\gamma\gamma}$ to $\mu_R = \mu_F = 2m_{W\gamma\gamma}$ increases the high p_T tail of the distribution by a factor 2.5 or more at NLO. In fact, in Fig. 4 for $\max p_T^j \simeq 100$ GeV, the scale-varied distributions intersect, which is yet another clear indication of the previously mentioned accidental stabilization of the vetoed cross section, which is cut dependent. In contrast, in Fig. 5, events with high invariant mass can be generated, where the high mass has its origin purely in the leptonic sector. These events can have two fairly soft jets which are not cut away, which yields smaller variations in the K -factor, with changes up to a factor 1.3 when increasing $\mu_R = \mu_F$ by a factor 4.

IV. SUMMARY AND CONCLUSIONS

We have calculated the full NLO QCD corrections to the processes $p\bar{p} \rightarrow \ell^-\bar{\nu}_\ell\gamma\gamma + \text{jet} + X$ and $p\bar{p} \rightarrow \ell^+\nu_\ell\gamma\gamma + \text{jet} + X$. All off-shell and finite width effects have been properly taken into account. This is the first NLO computation which falls into the three gauge boson-plus-jet category.

Quite typical for the multiboson+jet production modes we find large total K factors of order 1.4 for inclusive production, which are driven by additional jet radiation being significant for our inclusively chosen cuts. This enhancement is considerably larger than naive expectations from a LO scale variation. The corrections exhibit a non-trivial phase space dependence, which could easily be misinterpreted as non-Standard Model physics unless the differential QCD corrections are properly included in experimental analyses.

Acknowledgments

F.C. acknowledges partial support by FEDER and Spanish MICINN under grant FPA2008-02878. CE thanks Michael Spannowsky for many helpful discussions. This research is partly funded by the Deutsche Forschungsgemeinschaft under SFB TR-9 “Computergestützte Theoretische Teilchenphysik”, and the Helmholtz alliance “Physics at the Terascale”.

-
- [1] V. Hankele and D. Zeppenfeld, Phys. Lett. B **661** (2008) 103, T. Binoth, G. Ossola, C. G. Papadopoulos and R. Pittau, JHEP **0806** (2008) 082, F. Campanario, V. Hankele, C. Oleari, S. Prestel and D. Zeppenfeld, Phys. Rev. D **78** (2008) 094012, G. Bozzi, F. Campanario, V. Hankele and D. Zeppenfeld, Phys. Rev. D **81** (2010) 094030, G. Bozzi, F. Campanario, M. Rauch, H. Rzehak and D. Zeppenfeld, Phys. Lett. **B696**, 380-385 (2011).
 - [2] G. Bozzi, F. Campanario, M. Rauch and D. Zeppenfeld, Phys. Rev. D **83** (2011) 114035.
 - [3] J. Ohnemus, Phys. Rev. D **44** (1991) 1403, J. Ohnemus, Phys. Rev. D **44** (1991) 3477, J. Ohnemus, Phys. Rev. D **47** (1993) 940.
 - [4] J. M. Campbell, R. K. Ellis and C. Williams, arXiv:1105.0020 [hep-ph].
 - [5] V. Del Duca, F. Maltoni, Z. Nagy and Z. Trocsanyi, JHEP **0304** (2003) 059, S. Dittmaier, S. Kallweit

- and P. Uwer, Phys. Rev. Lett. **100**, 062003 (2008), J. M. Campbell, R. Keith Ellis and G. Zanderighi, JHEP **0712** (2007) 056, S. Dittmaier, S. Kallweit and P. Uwer, Nucl. Phys. B **826**, 18 (2010), T. Binoth, T. Gleisberg, S. Karg, N. Kauer and G. Sanguinetti, Phys. Lett. B **683** (2010) 154, S. Ji-Juan, M. Wen-Gan, Z. Ren-You and G. Lei, Phys. Rev. D **81** (2010) 114037.
- [6] F. Campanario, C. Englert, M. Spannowsky and D. Zeppenfeld, Europhys. Lett. **88**, 11001 (2009).
- [7] F. Campanario, C. Englert and M. Spannowsky, Phys. Rev. **D83**, 074009 (2011).
- [8] F. Campanario, C. Englert, S. Kallweit, M. Spannowsky and D. Zeppenfeld, JHEP **1007** (2010) 076,
- [9] M. Rubin, G. P. Salam and S. Sapeta, JHEP **1009** (2010) 084.
- [10] K. Arnold *et al.*, Comput. Phys. Commun. **180** (2009) 1661.
- [11] K. Hagiwara and D. Zeppenfeld, Nucl. Phys. B **313** (1989) 560.
- [12] J. Alwall *et al.*, JHEP **0709** (2007) 028.
- [13] H. Murayama, I. Watanabe and K. Hagiwara, KEK-Report 91-11, 1992.
- [14] B. Jager, C. Oleari and D. Zeppenfeld, JHEP **0607** (2006) 015; B. Jager, C. Oleari and D. Zeppenfeld, Phys. Rev. D **73**, 113006 (2006); G. Bozzi, B. Jager, C. Oleari and D. Zeppenfeld, Phys. Rev. D **75** (2007) 073004.
- [15] F. Campanario, arXiv:1105.0920 [hep-ph].
- [16] R. Mertig, M. Bohm and A. Denner, Comput. Phys. Commun. **64** (1991) 345.
- [17] T. Hahn, Comput. Phys. Commun. **140** (2001) 418,
- [18] T. Figy, C. Oleari and D. Zeppenfeld, Phys. Rev. D **68** (2003) 073005, C. Oleari and D. Zeppenfeld, Phys. Rev. D **69** (2004) 093004.
- [19] F. Campanario, C. Englert and M. Spannowsky, Phys. Rev. D **82** (2010) 054015.
- [20] C. Englert, B. Jager and D. Zeppenfeld, JHEP **0903** (2009) 060.
- [21] A. Denner, S. Dittmaier, M. Roth, and D. Wackeroth, Nucl. Phys. B **560** (1999), 33, C. Oleari and D. Zeppenfeld, Phys. Rev. D **69** (2004), 093004.
- [22] T. Hahn and M. Perez-Victoria, Comput. Phys. Commun. **118** (1999) 153.
- [23] T. Hahn and M. Rauch, Nucl. Phys. Proc. Suppl. **157**, 236 (2006) [arXiv:hep-ph/0601248].
- [24] G. Passarino and M. J. G. Veltman, Nucl. Phys. B **160**, 151 (1979).
- [25] A. Denner and S. Dittmaier, Nucl. Phys. B **658** (2003) 175, A. Denner and S. Dittmaier, Nucl. Phys. B **734** (2006) 62.
- [26] M. Ciccolini, A. Denner and S. Dittmaier, Phys. Rev. D **77** (2008) 013002, A. Bredenstein, A. Denner, S. Dittmaier and S. Pozzorini, JHEP **0808** (2008) 108, A. Bredenstein, A. Denner, S. Dittmaier and S. Pozzorini, Phys. Rev. Lett. **103** (2009) 012002, A. Bredenstein, A. Denner, S. Dittmaier and S. Pozzorini, JHEP **1003** (2010) 021, A. Denner, S. Dittmaier, S. Kallweit and S. Pozzorini, Phys. Rev. Lett. **106** (2011) 052001.
- [27] G. Bevilacqua, M. Czakon, C. G. Papadopoulos, R. Pittau and M. Worek, JHEP **0909** (2009) 109, G. Bevilacqua, M. Czakon, C. G. Papadopoulos and M. Worek, Phys. Rev. Lett. **104** (2010) 162002, G. Bevilacqua *et al.*, Nucl. Phys. Proc. Suppl. **205-206**, 211 (2010), JHEP **1102**, 083 (2011).
- [28] S. Catani and M. H. Seymour, Nucl. Phys. B **485** (1997) 291 [Erratum-ibid. B **510** (1998) 503].
- [29] H. L. Lai, M. Guzzi, J. Huston, Z. Li, P. M. Nadolsky, J. Pumplin and C. P. Yuan, Phys. Rev. D **82**, 074024 (2010)
- [30] J. Pumplin, D. R. Stump, J. Huston, H. L. Lai, P. Nadolsky, and W. K. Tung, JHEP **0207** (2002), 012.
- [31] S. Frixione, Phys. Lett. B **429** (1998) 369.
- [32] U. Baur, T. Han and J. Ohnemus, Phys. Rev. D **48** (1993) 5140.
- [33] M. Escalier *et al.*, CERN-ATL-PHYS-PUB-2005-018.
- [34] S. Hoeche, S. Schumann and F. Siegert, Phys. Rev. D **81** (2010) 034026.
- [35] U. Baur, D. Wackeroth and M. M. Weber, PoS **RAD-COR2009** (2010) 067.
- [36] S. Catani, Y. L. Dokshitzer, M. H. Seymour, and B. R. Webber, Nucl. Phys. B **406** (1993), 187, S. D. Ellis and D. E. Soper, Phys. Rev. D **48** (1993) 3160.